Optics Letters

Realization of a 101 W single-frequency continuous wave all-solid-state 1064 nm laser by means of mode self-reproduction

Yongrui Guo,[1,3] Minzhi Xu,[1] Weina Peng,[1] Jing Su,[1,2] Huadong Lu,[1,2,*] and Kunchi Peng[1,2]

[1]State Key Laboratory of Quantum Optics and Quantum Optics Devices, Institute of Opto-Electronics, Shanxi University, Taiyuan 030006, China
[2]Collaborative Innovation Center of Extreme Optics, Shanxi University, Taiyuan, Shanxi 030006, China
[3]e-mail: gyr_ls@163.com
*Corresponding author: luhuadong@sxu.edu.cn

Received 5 October 2018; accepted 7 November 2018; posted 15 November 2018 (Doc. ID 347576); published 11 December 2018

We realized a 101 W single-frequency continuous wave (CW) all-solid-state 1064 nm laser by means of mode self-reproduction in this Letter. Two identical laser crystals were placed into a resonator to relax the thermal lens of the laser crystals, and an imaging system was employed to realize cavity mode self-reproduced at the places of the laser crystals. Single-frequency operation of the resonator was realized by employing a new kind of high extinction ratio optical diode based on the terbium scandium aluminum garnet crystal to realize a stable unidirectional operation of the laser, together with introducing a large enough nonlinear loss to the resonator to effectively suppress the multi-mode oscillation and mode hopping of the laser. As a result, a 101 W single-frequency 1064 nm laser in a single-ring resonator was achieved with 42.3% optical efficiency. The measured power stability for 8 h and the beam quality were better than ±0.73% and 1.2, respectively.

https://doi.org/10.1364/OL.43.006017

Single-frequency continuous wave (CW) solid-state lasers with excellent output performances, including perfect beam quality, high stability, and low intensity noise have important and widespread applications in scientific research and high-tech fields of quantum optics and quantum information, atom physics, and high-precision measurements. In particular, the successful observation of the gravitational wave on September 14, 2015 [1], made the high-power single-frequency CW laser become a star, since it played a major role in the laser-based Michelson interferometers and helped humans to precisely observe and study the universe. To date, several techniques have been developed for the realization of single-frequency laser, including a monolithic non-planar ring oscillator in a magnetic field [2], short cavity with Fabry–Perot (F-P) etalon, ring cavity with an optical diode (OD) [3], etc. Compared to other techniques, a ring resonator, combined with an OD and other mode-selected elements, was an effective method to achieve a highly stable single-frequency laser with high output power and perfect mode quality. Because both the spatial hole burning effect and the non-lasing oscillation of the laser can be effectively eliminated. In recent years, a large amount of work has been done to scale up the optical power and improve the beam quality of the single-frequency all-solid-state laser, such as direct pumping technology [4], dual-end pumping scheme, adopting a composite laser crystal [3], employing a low-doped laser crystal with long length, self-compensating the astigmatism of the laser [4], and active compensation of the thermal lens effect with a negatively thermal-optical crystal [5]. In addition, for ensuring the single-longitudinal-mode (SLM) characteristic of the laser with the high output power, a method of introducing a nonlinear loss to a unidirectional resonator was developed [6], where loss difference between the lasing mode and side non-lasing modes can effectively suppress the oscillation of the non-lasing modes [7]. Up to now, a stable single-frequency 1064 nm laser with the highest output power of 50.3 W had been achieved, which was realized by a combination of a direct pumping scheme, composite laser crystal, and astigmatism self-compensation with the nonlinear loss [8]. While the output power of the single-frequency laser was further being scaled up by only increasing the pump power of the laser crystal, the harmful thermal lens effect of the laser crystal dramatically narrowed the stable range of the laser. What is more serious is that high pump power can cause high risks of crystal fracture. In order to relax the thermal lens effect and damage pressure of the single-laser crystal, as well as effectively compensate for the thermal refractive power, inserting more than one laser crystals and picking designated lenses into a single resonator paved an effective way to attain the high output power. In 2011, Xie *et al.* reported a single-frequency side-pumped Nd:YAG ring laser with two pieces of laser crystals. However, the output power was restricted to 31.9 W [9]. High-power single-frequency lasers using injection locking [10] or a master oscillator power amplifier with several laser crystals were also constructed and demonstrated [11], but the laser systems were very complex and expensive. In this Letter, we presented a mode self-reproduced 101 W single-frequency CW all-solid-state 1064 nm laser. Two identical laser crystals were placed into a ring resonator, and an imaging system was used to implement the mode self-reproduction. Stable SLM operation of the

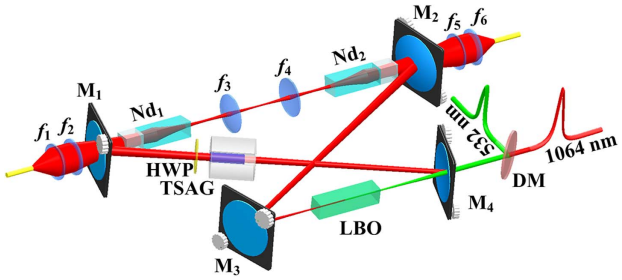

Fig. 1. Schematic of the experimental setup. TSAG, terbium scandium aluminum garnet; $Nd_{1\text{-}2}$, YVO_4/Nd:YVO_4; LBO, lithium triborate; HWP, half-wave plate; DM, dichroic mirror; $f_{1\text{-}6}$, lens.

single-frequency laser was attained by the combination of a new kind of OD with a high extinction ratio and introducing large enough nonlinear loss to the resonator. To the best of our knowledge, this is the highest output power in a single all-solid-state single-frequency laser resonator.

The schematic of the designed single-frequency 1064 nm laser was depicted in Fig. 1. A symmetrical bow-tie cavity containing two identical laser crystals and an imaging system were constructed. Both of the laser crystals were a-cut composite YVO_4/Nd:YVO_4 rods, which had an undoped end cap of 3 mm and an Nd-doped part of 20 mm with a concentration of 0.8% and a wedge angle of 1.5 deg at the second end face to suppress the σ-polarization oscillation and enhance the superiority of the π-polarization mode. The front end face of the YVO_4/Nd:YVO_4 crystal was coated with anti-reflection (AR) films at 1064 and 888 nm ($R_{1064\,\mathrm{nm};888\,\mathrm{nm}} < 0.25\%$), and the second end face was coated with AR films at 1064 nm ($R_{106\,\mathrm{nm}} < 0.25\%$). In order to precisely control the temperature of two laser crystals, both of them were wrapped with indium foil and enclosed by water-cooled copper blocks adhered with a thermoelectric cooler for heat dissipation. Two laser crystals were separately pumped with two identical fiber-coupled laser diodes (LDs) with the center wavelength of 888 nm. The spectral bandwidth and the maximum output power of both LDs were 3.56 nm and 120 W, respectively. The diameter and the numerical aperture of the coupling fibers were 400 μm and 0.22, respectively. Both of the pump radiations were imaged to a 1140 μm diameter pump spot in the center of the laser crystals. The input couplers M_1 and M_2 were two identical concave–convex mirrors with curvature radii of $R = 1500$ mm, which were coated with high-transmission (HT) films at 888 nm ($T_{888\,\mathrm{nm}} > 99.5\%$) and high-reflection (HR) films at 1064 nm ($R_{1064\,\mathrm{nm}} > 99.7\%$), respectively. M_3 and M_4 were two plane–concave mirrors with a curvature radii of $R = -100$ mm, where M_3 was coated with HR films at 1064 nm, and the output coupler M_4 was coated with partial transmission at 1064 nm and HT films at 532 nm. An imaging system composed of two identical plane-convex lenses (f_3, f_4, $f = 100$ mm) was inserted between the two laser crystals for realizing the self-reproduction of the cavity mode at each laser crystal. The optical length between the main plane of each laser crystal, and their adjacent imaging lens was set to 100 mm. In addition, the optical length between the two imaging lenses was actively changed in the experiment to adapt the thermal lens effect of both laser crystals, as well as to shift the stability working point (SWP) of the laser to a high pump power region. To completely eliminate the spatial hole burning effect and realize a stable unidirectional operation of the laser, a new kind of OD with a high extinction ratio was employed. It was composed of a 7 mm long terbium scandium aluminum garnet (TSAG) crystal (Castech, Inc.) and a half-wave plate. Compared to the common terbium gallium garnet (TGG) crystal, TSAG crystal possessed superiority, including a larger Verdet constant of 48 rad T^{-1} m^{-1} (about 25% higher than that of TGG) and a low absorption with less than 3000 ppm$(cm)^{-1}$ at 1064 nm (about 33% less than that of TGG). According to Ref. [12], a high isolation ratio of 35.7 dB for the TSAG-based Faraday isolator was attained with a radiation power as high as 1440 W. In order to effectively suppress the non-lasing mode oscillation of the laser, a type-I non-critically phase-matched lithium triborate (LBO) crystal (S1, S2: $AR_{1064\,\mathrm{nm};532\,\mathrm{nm}}$) with the dimensions of 3 mm × 3 mm × 18 mm was employed to introduce nonlinear loss into the cavity due to its high damage threshold, absence of walk-off, as well as larger temperature and angular acceptances. The nonlinear LBO crystal was placed at the beam waist between M_3 and M_4, and its temperature was controlled by a home-made temperature controller with the precision of 0.01°C. A dichroic mirror separated the output of 532 nm laser from that of a 1064 nm laser. The output powers of 532 and 1064 nm laser were separately monitored by the power meter (LabMax-Top, Coherent) with an uncertainty of ±1%.

In order to extract as much output power as possible, the overlap between the pump beams and laser modes had to be optimized, while the overall pump power was being injected into the resonator. Consequently, the distance between two imaging lenses had to be precisely calculated according to the thermal focal-length variation and manipulated in the process of the experiment. Simultaneously, the relationships between the SWP of the laser, the distance of two imaging lenses and the thermal lenses of both laser crystals were numerically simulated by using an ABCD matrix formalism. According to the calculation, the SWP of the laser can shift to the full pump power of 120 W per end by optimizing the distance between the two imaging lenses to 108 mm with respect to a total cavity length of 948 mm. In this case, the beam diameter inside the oscillator was obtained and depicted in Fig. 2. It was clear that when the full pump light of 120 W per end was used to pump the laser crystals, both of the beam waists at the places of two laser crystals were 470 μm, which revealed that the distance of 108 mm between two imaging lenses was enough to realize the mode self-reproduction. At this moment, the achieved pump-to-mode size ratio was 1.21, which satisfied the mode-matching condition presented by Chen [13].

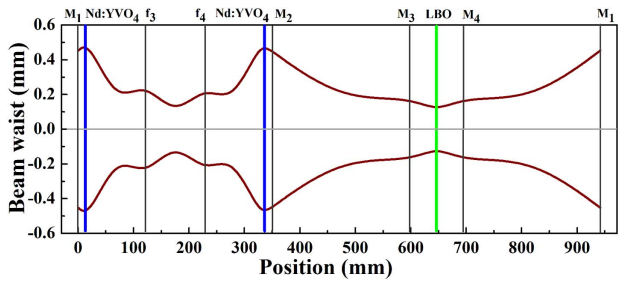

Fig. 2. Beam diameter inside the optimized oscillator.

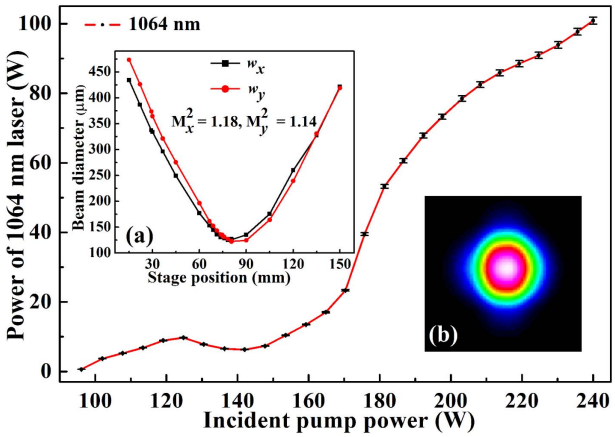

Fig. 3. Output power of a 1064 nm laser versus the incident pump power. The insets are (a) the beam quality factor and (b) the profile of a 1064 nm laser at the maximum output power.

In the experiment, the output coupling was optimized by employing an output coupler M_4 coated with the transmission of 37% at 1064 nm wavelength based on the accurate measurement method of the intra-cavity linear loss of lasers by means of the nonlinear loss [14]. By controlling the temperature of the LBO crystal to the optimal phase-matching temperature of 149.0°C, the output power of 1064 nm laser as a function of the incident pump power was plotted, as shown in Fig. 3. This illustrated that the lasing threshold power was around 96.12 ± 0.96 W; the highest output power of the single-frequency 1064 nm laser reached 101.00 ± 1.00 W with the overall incident pump power of 240 W. Owing to the existence of the nonlinear LBO crystal, a single-frequency 532 nm laser beam with the maximal output power of 1.91 ± 0.02 W was simultaneously generated. The overall optical-to-optical conversion efficiency achieved was as high as 42.3%. It was clear that the overall pump power of 240 W was completely injected into the resonator, and the SWP of the resonator was well matched with the maximum pump power of the LDs. In order to achieve more output power of the laser, a higher pump power of the LDs should be employed, together with the new design of a suitable laser structure. In Fig. 3, the drop-in output power between 125 and 150 W pump power can be attributed to two factors. On one hand, a slightly different absorption in the laser crystals resulted from the wavelength shift of the LDs with the change of the diode current causing a waist size difference between both laser crystals, which worsened the overlap between the pump beam and the laser mode inside the laser crystals. On the other hand, along with increasing the pump power, the changed thermal refractive power resulted in the symmetry axis running between f_3 and f_4 and M_3 and M_4, respectively, leading to variable thermal lenses that are not centered. Additionally, the nonlinear characteristic of the output power curve was dramatic, which was ascribed to the nonlinear second-harmonic generation process. The beam quality of the 1064 nm laser was measured by a M^2 meter (M2SETVIS, Thorlabs) and the measured values of M_x^2 and M_y^2 were 1.18 and 1.14, respectively. The measured caustic curve and the corresponding spatial beam profile were shown as insets (a) and (b) in Fig. 3, respectively.

The potential of the implemented laser in terms of power scalability can also be calculated according to the oscillation condition of the single-frequency laser with intra-cavity nonlinear loss [14]. The gain of the implemented laser should be the sum of that generated by each laser crystal. Thereby, the intra-cavity FW power intensity (I) can be given by

$$I = \frac{\sqrt{(t+\delta-\eta I_s)^2 + 4\eta I_s (2g_0)l} - (t+\delta+\eta I_s)}{2\eta}, \quad (1)$$

where t was the transmission of the output coupler, η was the factor of the nonlinear conversion, δ represented the round-trip intra-cavity loss, I_s was the saturation power intensity, g_0 and l denoted the small-signal gain factor and the length of the laser crystals, respectively, and $g_0 l = KP_{in}$, while K and P_{in} were the factors of the pump and the per-end pump power, respectively.

The output power of the laser at FW (P_f) and second-harmonic wave (P_{sh}) were described as [14]

$$P_f = AIt, \quad (2)$$

$$P_{\mathrm{sh}} = A\eta I^2, \quad (3)$$

where A stood for the average transverse cross section of the laser beam in the laser crystal. To accurately estimate the output power of the designed laser, the pump factor $K = g_0 l/P_{in}$ was calculated via taking the influence of the energy transfer upconversion effect into account [15]. The calculated value of the pump factor K was 0.089 W^{-1}. By taking the laser parameters listed in Table 1 into Eqs. (1)–(3), the output powers at 1064 and 532 nm of the implemented laser were calculated to be 102.44 and 2.98 W, respectively. It can be concluded that the theoretical calculations were consistent with the experiment results, including the maximal output power of 101 and 1.91 W for 1064 and 532 nm, respectively.

The longitudinal-mode structure of the 1064 nm laser was monitored by scanning the confocal F-P cavity with a free spectral range of 750 MHz and finesse of 120, respectively. The transmission curve of the inset in Fig. 4 confirmed that the 1064 nm laser was stably running in SLM operation, revealing that the introduced nonlinear loss by the nonlinear LBO crystal was large enough to effectively suppress the multi-mode oscillation and mode hopping of the laser [6,8,14]. The long-term power stability of the 1064 nm laser was measured during an 8 h period. At the output power of 101 W, the power stability were better than ±0.73% and 0.17% for peak-to-peak power fluctuations and rms, respectively, as shown in Fig. 4. Thanks to the excellent thermal and mechanical properties of the TSAG crystal, the degree of the polarization of the 1064 nm laser reached 135:1, confirming that the 101 W single-frequency 1064 nm laser was linearly polarized.

The relative intensity noise (RIN) of the 1064 nm laser was measured by employing a homemade balanced homodyne detection with the common mode rejection ratio of 60 dB (Yuguang Co., Ltd.) [8]. At the detection power of 1 mW, for both of the InGaAs photodiodes (ETX500, JDSU Corporation), the measured RIN spectrum of the single-frequency 1064 nm laser reached the quantum noise limit [QNL, curve (a) of Fig. 4]

Table 1. Relevant Parameters of the Designed Laser

δ(%)	η (m^2/W)	I_s (W/m^2)	K (W^{-1})	A (mm^2)
5.5	2.7×10^{-11}	8.30827×10^6	0.089	0.694

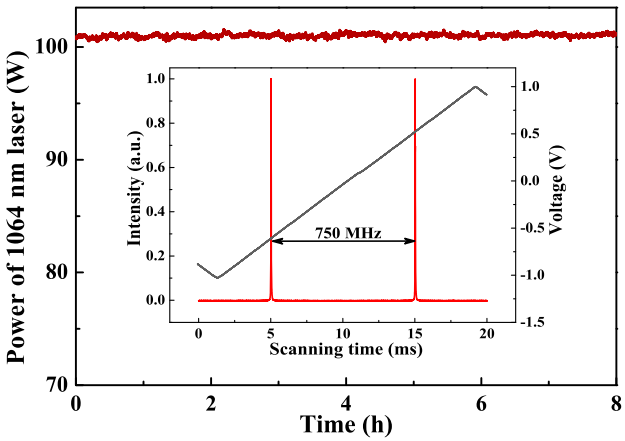

Fig. 4. Measured long-term power stability of a 101 W 1064 nm laser for 8 h. The inset shows the SLM structure of the laser.

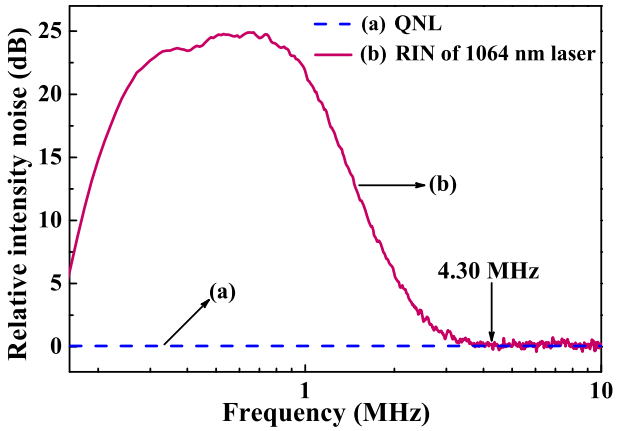

Fig. 5. Measured RIN of a 1064 nm laser. (a) QNL and (b) RIN spectrum of a 1064 nm laser.

at the frequency of 4.3 MHz, shown as curve (b) in Fig. 5. The linewidth of the single-frequency 1064 nm laser was also measured by employing a delayed self-heterodyne interferometer with a path length imbalance of 25 km between long and short branches of the interferometer [8]. The measured self-heterodyne linewidth data [curve (a) in Fig. 6] was fitted by the Gaussian lineshape function. The fitted result shown as curve (b) in Fig. 6 illustrated that the measured spectral linewidth of the 1064 nm laser was 365 kHz. Both measurement setups for measuring the RIN and the linewidth of the laser were similar to those demonstrated in [8].

In summary, we realized a linearly polarized 101 W single-frequency CW 1064 nm laser with perfect beam quality, high stability, and low intensity noise. The employed laser structure was a bow-tie cavity with two identical Nd:YVO_4 crystals placed in a ring resonator and an imaging system for mode self-reproduction. High output power was achieved by actively shifting the SWP of the laser to a full pump power region of 120 W per end, which was realized in the experiment by precisely manipulating the distance between two imaging lenses according to the generated thermal focal lengths of two laser crystals and the overall cavity length. By utilizing the TSAG

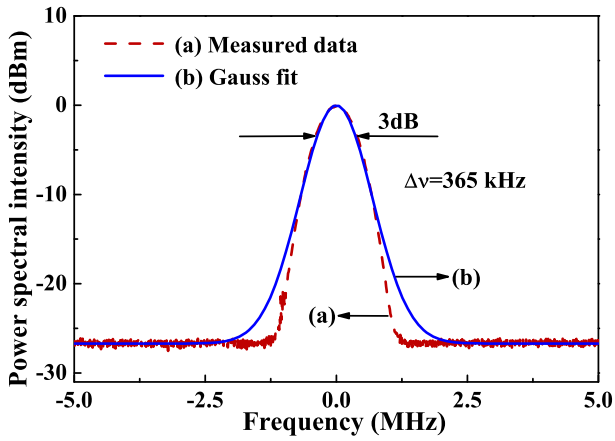

Fig. 6. (a) Measured self-heterodyne linewidth date with a 25 km delay fiber and (b) the Gaussian function fitting result of a 1064 nm laser.

OD and introducing the large enough nonlinear loss to the resonator, the stable SLM operation of the single-frequency laser was attained. When the total pump power was increased to 240 W, the maximal output power of a single-frequency 1064 nm laser reached 101 W. Accompanying the single-frequency 1064 nm laser beam, there was a 1.91 W 532 nm laser leaked from the resonator. The overall optical-to-optical conversion efficiency achieved as high as 42.3%. At the maximal output power of the laser, the high-power stability better than ±0.73%, perfect beam quality better than 1.2, and linewidth narrower than 365 kHz were simultaneously attained. The superior characteristics of the obtained laser will be applicable in the fields of quantum net, precise measurements, and so on. The presented design idea can also open a new way for further scaling up the optical power of the all-solid-state single-frequency laser.

Funding. Key Project of the Ministry of Science and Technology of the People's Republic of China (MOST) (2017YFB0405203).

REFERENCES

1. LIGO Scientific Collaboration and Virgo Collaboration, Phys. Rev. Lett. **116**, 061102 (2016).
2. T. J. Kane and R. L. Byer, Opt. Lett. **10**, 65 (1985).
3. J. Q. Zhao, Y. Z. Wang, B. Q. Yao, and Y. L. Ju, Laser Phys. Lett. **7**, 135 (2010).
4. Y. J. Wang, Y. H. Zheng, Z. Shi, and K. C. Peng, Laser Phys. Lett. **9**, 506 (2012).
5. Q. W. Yin, H. D. Lu, J. Su, and K. C. Peng, Opt. Lett. **41**, 2033 (2016).
6. H. D. Lu, J. Su, Y. H. Zheng, and K. C. Peng, Opt. Lett. **39**, 1117 (2014).
7. K. I. Martin, W. A. Clarkson, and D. C. Hanna, Opt. Lett. **22**, 375 (1997).
8. Y. R. Guo, H. D. Lu, M. Z. Xu, J. Su, and K. C. Peng, Opt. Express **26**, 21108 (2018).
9. S. Y. Xie, Y. Bo, J. L. Xu, Z. C. Wang, Q. J. Peng, D. F. Cui, and Z. Y. Xu, Chin. Phys. Lett. **28**, 084207 (2011).
10. A. Sträßer, T. Waltinger, and M. Ostermeyer, Appl. Opt. **46**, 8358 (2007).
11. C. Basu, P. Weßels, J. Neumann, and D. Kracht, Opt. Lett. **37**, 2862 (2012).
12. A. V. Starobor, I. L. Snetkov, and O. V. Palashov, Opt. Lett. **43**, 3774 (2018).
13. Y. F. Chen, J. Opt. Soc. Am. B **17**, 1835 (2000).
14. Y. R. Guo, H. D. Lu, Q. W. Yin, and J. Su, Chin. Opt. Lett. **15**, 021402 (2017).
15. X. Délen, F. Balembois, and P. Georges, J. Opt. Soc. Am. B **29**, 2339 (2012).